Electronic Supplementary Information

A novel conception for spontaneous transversions caused by homo-pyrimidine DNA mismatches: QM/QTAIM highlight

Ol'ha O. Brovarets'[a,b] & Dmytro M. Hovorun[a,b,✉]

[a]Department of Molecular and Quantum Biophysics, Institute of Molecular Biology and Genetics, National Academy of Sciences of Ukraine, 150 Akademika Zabolotnoho Str., 03680 Kyiv, Ukraine

[b]Department of Molecular Biotechnology and Bioinformatics, Institute of High Technologies, Taras Shevchenko National University of Kyiv, 2-h Akademika Hlushkova Ave., 03022 Kyiv, Ukraine

✉Corresponding author. E-mail: dhovorun@imbg.org.ua

1. Computational Details.

All calculations of the geometries and harmonic vibrational frequencies of the considered base mispairs and transition states of their conversion have been performed using Gaussian'09 package [1] at the DFT(B3LYP)/6-311++G(d,p) level of theory [2-4], that has been established to be a very good compromise between computational effort and accuracy and verified to give accurate geometrical structures, normal mode frequencies, barrier heights and characteristics of intermolecular H-bonds [5,6]. A scaling factor that is equal to 0.9668 has been applied in the present work for the correction of the harmonic frequencies of all studied base pairs [7-9]. We have confirmed the minima and TSs, located by means of Synchronous Transit-guided Quasi-Newton method [10], on the potential energy landscape by the absence or presence, respectively, of the imaginary frequency in the vibrational spectra of the complexes.

In order to consider electronic correlation effects as accurately as possible, we followed geometry optimizations with single point energy calculations using MP2 level of theory [11] and a wide variety of basis sets, in particular, Pople's basis sets of valence triple-ζ quality [12,13], as well as Dunning's cc-type basis sets [14], augmented with polarization and/or diffuse functions: 6-311++G(2df,pd), 6-311++G(3df,2pd), cc-pVTZ and cc-pVQZ.

Reaction pathways have been established by following intrinsic reaction coordinate (IRC) in the forward and reverse directions from each TS using Hessian-based predictor-corrector integration algorithm [15] with tight convergence criteria. These calculations eventually ensure that the proper reaction pathway, connecting the expected reactants and

products on each side of the TS, has been found. We've have investigated the evolution of the energetic and geometric characteristics of the H-bonds and base pairs along the reaction pathway establishing them at each point of the IRC [16,17].

Electronic interaction energies E_{int} have been calculated at the MP2/6-311++G(2df,pd) level of theory as the difference between the total energy of the base mispair and the energies of the isolated monomers. Gibbs free energy of interaction has been obtained using similar equation. In each case the interaction energy was corrected for the basis set superposition error (BSSE) [18,19] through the counterpoise procedure [20,21].

The Gibbs free energy G for all structures was obtained in the following way:

$$G=E_{el}+E_{corr}, \quad (1)$$

where E_{el} – electronic energy, while E_{corr} – thermal correction. We applied the standard TS theory [22] to estimate the activation barriers of the tautomerisation reaction.

The time $\tau_{99.9\%}$ necessary to reach 99.9% of the equilibrium concentration of the reactant and product in the system of reversible first-order forward (k_f) and reverse (k_r) reactions can be estimated by formula [22]:

$$\tau_{99.9\%} = \frac{ln10^3}{k_f + k_r}. \quad (2)$$

The rate constants k_f and k_r were estimated by the formula [22]:

$$k_{f,r} = \frac{k_B \cdot T}{h} \cdot e^{-\frac{\Delta\Delta G_{f,r}}{RT}}, \quad (3)$$

where k_B – Boltzmann's constant, h – Planck's constant, $\Delta\Delta G_{f,r}$ – Gibbs free energy of activation for the tautomerisation reaction in the forward (*f*) and reverse (*r*) directions, v_i – magnitude of the imaginary frequency in the TSs.

Bader's quantum theory of Atoms in Molecules (QTAIM) was applied to analyse the electron density distribution [24-27]. The topology of the electron density was analysed using program package AIMAll [28] with all default options. The presence of a bond critical point (BCP), namely the so-called (3,-1) BCP, and a bond path between hydrogen donor and acceptor, as well as the positive value of the Laplacian at this BCP ($\Delta\rho>0$), were considered as criteria for the H-bond formation [29,30]. Wave functions were obtained at the level of theory used for geometry optimisation.

The energies of the specific N3H···HN4 and attractive O/N···O van der Waals contacts [29-31] in the base mispairs and TSs of their interconversion *via* the sequential DPT were calculated by the empirical Espinosa-Molins-Lecomte (EML) formula [31,33] based on the electron density distribution at the (3,-1) BCPs of the contacts:

$E_{N3H\cdots HN4\,/\,O/N\cdots O}$=0.5·V(r), (4)

where V(r) – value of a local potential energy at the (3,-1) BCP.

The energies of all AH···B conventional H-bonds were evaluated by the empirical Iogansen's formula [34]:

$E_{AH\cdots B} = 0.33\cdot\sqrt{\Delta\nu - 40}$, (5)

where Δν – magnitude of the frequency shift of the stretching mode of the AH H-bonded group involved in the AH···B H-bond relatively the unbound group. The partial deuteration was applied to minimize the effect of vibrational resonances [6-8].

The energy of the O4H···N3 H-bond in the $TS_{T\cdot T(w)\leftrightarrow T^*\cdot T^*O2(w)}$ and N4H···N4 H-bond in the $TS_{C^*\cdot C^*(w)\leftrightarrow C^*O2\cdot C(w)}$, respectively, containing loosened covalent bridges were estimated by the Nikolaienko-Bulavin-Hovorun formulas [35]:

$E_{O4H\cdots N3}$=1.72 + 142·ρ, (6)

$E_{N4H\cdots N4}$=-2.03+225·ρ, (7)

where ρ – the electron density at the (3,-1) BCP of the H-bond.

The atomic numbering scheme for the DNA bases is conventional [36].

2. Numerical and Graphical Materials.

Table S1. Electron-topological, structural, vibrational and energetic characteristics of the intermolecular H-bonds and attractive van der Waals contacts in the DNA homo-pyrimidine mispairs containing C and T nucleobases and TSs of their tautomerisation *via* the sequential DPT and structural displacement of the bases relatively to each other, energetic and polar characteristics of the latters obtained at the B3LYP/6-311++G(d,p) level of theory.

Base pair/TS	AH···B H-bond/ O/N···O van der Waals contact	ρ^a	$\Delta\rho^b$	$100\cdot\varepsilon^c$	$d_{A\cdots B/O/N\cdots O}{}^d$	$d_{H\cdots B}{}^e$	$\Delta d_{AH}{}^f$	∠AH···B^g	$\Delta\nu^h$	$E_{AH\cdots B/O/N\cdots O}{}^i$	ΔG^j	μ^k
T·T(w)	N3H···O4	0.029	0.103	2.82	2.887	1.872	0.017	168.1	279.3	5.11	0.00	1.22
	N3H···O2	0.029	0.104	3.85	2.886	1.868	0.016	169.6	273.4	5.04		
T·T*(w)[37]	O4H···O4	0.050	0.144	2.01	2.641	1.645	0.031	172.9	599.9	7.81	8.98	2.71
	N1H···N1	0.027	0.077	6.21	3.004	1.998	0.021	163.5	359.3	5.90		
	O2···O2	0.002	0.008	30.35	3.756	-	-	-	-	0.29*		
T*$_{O2}$·T(WC)	O4···O4	0.002	0.007	60.45	3.808	-	-	-	-	0.25*	12.72	5.35
	N3H···N3	0.027	0.076	5.96	3.001	2.002	0.022	161.4	363.0	5.93		
	O2H···O2	0.052	0.149	2.68	2.620	1.620	0.034	175.3	656.6	8.19		
TS$_{T\cdot T(w)\leftrightarrow T^*\cdot T^*O2(w)}$	O4H···N3	0.108	0.011	4.07	2.533	-	-	-	-	17.01**	13.82	1.74
TS$_{T^*O2\cdot T(w)\leftrightarrow T\cdot T^*O2(WC)}$	O4···O4	0.003	0.011	10.06	3.538	-	-	-	-	0.54*	17.11	4.64
T*·T*$_{O2}$(w)	O4H···N3	0.063	0.094	4.90	2.660	1.631	0.059	179.1	1096.9	10.73	15.61	1.57
	O2H···N3	0.068	0.091	5.02	2.640	1.606	0.066	179.4	1215.4	11.31		
TS$^{T+\cdot T-}{}_{T\cdot T(w)\leftrightarrow T\cdot T^*(WC)}$	O4$^+$H···O4$^-$	0.036	0.094	10.73	2.712	1.818	0.053	143.8	879.7	5.34	31.06	6.96
	O4$^+$H···N3$^-$	0.029	0.084	28.05	2.836	1.947	0.053	143.7	879.7	4.22		
	N3$^+$H···N3$^-$	0.020	0.070	28.45	2.951	2.121	0.029	134.5	462.3	3.02		
	N3$^+$H···O2$^-$	0.025	0.075	7.43	2.972	1.973	0.029	158.5	462.3	3.76		
TS$^{T-\cdot T+}{}_{T\cdot T(w)\leftrightarrow T^*O2\cdot T(WC)}$	N3$^+$H···O4$^-$	0.031	0.085	1.88	2.909	1.887	0.037	162.4	592.1	4.84	32.82	6.49
	N3$^+$H···N3$^-$	0.020	0.070	52.60	2.934	2.139	0.037	130.4	592.1	2.92		
	O2$^+$H···N3$^-$	0.028	0.085	52.67	2.824	1.979	0.055	137.9	922.4	3.80		
	O2$^+$H···O2$^-$	0.040	0.100	7.55	2.687	1.759	0.055	148.6	922.4	6.00		
C·C*(WC)[38]	N4H···N4	0.034	0.090	6.63	2.925	1.895	0.025	174.3	447.4	6.66	0.00	4.87
	N3H···N3	0.030	0.081	6.39	2.982	1.950	0.024	173.0	423.8	6.47		
	O2···O2	0.002	0.008	21.69	3.721	-	-	-	-	0.33*		
C*·C*(w)	N3H···N4	0.038	0.094	6.34	2.884	1.849	0.030	171.8	520.5	7.23	1.34	1.08
	N3H···O2	0.028	0.100	4.25	2.906	1.883	0.017	172.7	281.7	5.13		
C*$_{O2}$·C(w)	N4H···N3	0.039	0.098	6.64	2.864	1.838	0.027	170.4	482.2	6.94	7.40	1.45
	O2H···N3	0.058	0.094	5.53	2.692	1.670	1.024	176.1	1109.2	10.79		
C·C(w)	N4H···N3	0.018	0.054	8.23	3.193	2.190	0.012	167.5	-	4.11	8.90	10.66
	N3···O2	0.001	0.005	20.63	4.047	-	-	-	-	0.16*		
TS$^{C-\cdot C+}{}_{C\cdot C^*(WC)\leftrightarrow C^*\cdot C^*(w)}$	N4$^+$H···N4$^-$	0.035	0.089	1.66	2.855	1.871	0.037	155.0	1300.2	11.71	18.34	7.71
	N4$^+$H···N3$^-$	0.021	0.072	36.54	2.950	2.108	0.037	135.7	1300.2	11.71		
	N3$^+$H···N3$^-$	0.019	0.063	22.79	3.025	2.149	0.030	140.0	1241.6	11.44		
	N3$^+$H···O2$^-$	0.022	0.068	9.78	3.001	2.025	0.030	154.3	1241.6	11.44		
TS$^{C-\cdot C+}{}_{C\cdot C(w)\leftrightarrow C\cdot C^*(WC)}$	N4$^+$H···N4$^-$	0.029	0.094	7.30	2.825	1.943	0.015	142.3	193.0	4.08	34.28	13.26
	N3$^+$H···N4$^-$	0.062	0.079	6.16	2.711	1.660	0.088	157.2	1248.1	11.47		
	N3$^+$···O2$^-$	0.005	0.014	9.15	3.424	-	-	-	-	0.84*		

[a]The electron density at the (3,-1) BCP of the H-bond, a.u.; [b]The Laplacian of the electron density at the (3,-1) BCP of the H-bond, a.u.; [c]The ellipticity at the (3,-1) BCP of the H-bond; [d]The distance between the A (H-bond donor) and B (H-bond acceptor) atoms of the AH···B H-bond, Å; [e]The distance between the H and B atoms of the AH···B H-bond, Å; [f]The elongation of the H-bond donating group AH upon the AH···B H-bonding, Å; [g]The H-bond angle, degree; [h]The redshift of the stretching vibrational mode ν(AH) of the AH H-bonded group, cm^{-1}; [i]Energy of the H-bonds calculated by Iogansen's formula [34], the O2/4/N3···O2/4 van der Waals contacts – by Espinose-Molins-Lecomte formula (marked with an asterisk) [32,33] and the N/O4H···N3/4 H-bonds in the TS – by Nikolaienko-Bulavin-Hovorun formulas (marked with double asterisk) [35], kcal·mol^{-1}; [j]The relative Gibbs free energy of the complex obtained at the MP2/cc-pVQZ//B3LYP/6-311++G(d,p) level of theory under normal conditions, kcal·mol^{-1}; [k]The dipole moment of the complex, D.

Table S2. Energetic characteristics of the investigated DNA base pairs and steps of the tautomerization via the sequential DPT[38] obtained at the different levels of theory for the geometry calculated at the B3LYP/6-311++G(d,p) level of theory.

Complex	Level of theory							
	MP2/6-311++G(3df,pd)		MP2/6-311++G(3df,2pd)		MP2/cc-pVTZ		MP2/cc-pVQZ	
	ΔG^a	ΔE^b	ΔG^a	ΔE^b	ΔG^a	ΔE^b	ΔG^a	ΔE^b
T·T(w)	0.00	0.00	0.00	0.00	0.00	0.00	0.00	0.00
T·T*(WC)[37]	8.82	8.49	9.18	8.85	8.76	8.43	8.98	8.64
T^*_{O2}·T(WC)	12.68	12.77	12.91	13.00	12.57	12.66	12.72	12.81
$TS_{T·T*(WC)↔T*·T(WC)}$[37]	12.79	15.97	13.65	16.84	13.11	16.29	13.63	16.82
$TS_{T·T(w)↔T*·T*O2(w)}$	13.14	16.34	13.89	17.10	13.47	16.68	13.82	17.03
$T^*·T^*_{O2}(w)$	15.17	15.55	15.77	16.15	15.36	15.74	15.61	15.99
$TS_{T*O2·T(WC)↔T·T*O2(WC)}$	16.42	19.68	17.15	20.41	16.67	19.92	17.11	20.37
C·C*(WC)[38]	0.00	0.00	0.00	0.00	0.00	0.00	0.00	0.00
C*·C*(w)	1.61	1.77	1.31	1.47	1.28	1.44	1.34	1.50
C^*_{O2}·C(w)	7.42	7.88	7.45	7.91	7.48	7.93	7.40	7.86

[a]The relative Gibbs free energy of the investigated complexes ($\Delta G_{T·T(w)/C·C*(WC)}$=0.00; T=298.15 K), kcal·mol^{-1}

[b]The relative electronic energy of the investigated complexes ($\Delta E_{T·T(w)/C·C*(WC)}$=0.00), kcal·mol^{-1}

Table S3. Interbase interaction energies (in kcal·mol^{-1}) for the investigated DNA base mispairs and TSs of their conversions *via* the sequential DPT obtained at the MP2/6-311++G(3df,2pd)//B3LYP/6-311++G(d,p) level of theory.

Complex	$-\Delta E_{int}$[a]	ΣE_{HB}[b]	$\Sigma E_{HB}/\lvert\Delta E_{int}\rvert$, %	$-\Delta G_{int}$[c]
T·T(w)	12.03	10.15	84.3	0.56
T·T*(WC)[37]	16.67	14.00	84.0	4.69
T^*_{O2}·T(WC)	18.27	14.38	78.7	6.47
T*·T^*_{O2}(w)	32.00	22.04	68.9	20.39
$TS^{T+\cdot T-}_{T\cdot T(w)\leftrightarrow T\cdot T^*(WC)}$	129.14	16.34	12.7	117.64
$TS^{T-\cdot T+}_{T\cdot T(w)\leftrightarrow T^*O2\cdot T(WC)}$	132.26	17.56	13.3	120.56
C·C*(WC)[38]	14.75	13.46	91.2	2.34
C*·C*(w)	13.80	12.36	89.6	2.26
C^*_{O2}·C(w)	27.91	17.73	63.5	15.43
C·C(w)	2.50	4.27	170.6	0.79
$TS^{C-\cdot C+}_{C\cdot C^*(WC)\leftrightarrow C^*\cdot C^*(w)}$	123.17	23.15	18.8	111.30
$TS^{C-\cdot C+}_{C\cdot C(w)\leftrightarrow C\cdot C^*(WC)}$	113.00	16.39	14.5	100.81

[a]The BSSE-corrected electronic interaction energy

[b]The total energy of the specific intermolecular interactions – H-bonds and attractive van der Waals contacts (see Table S1)

[c]The BSSE-corrected Gibbs free energy of interaction (T=298.15 K)

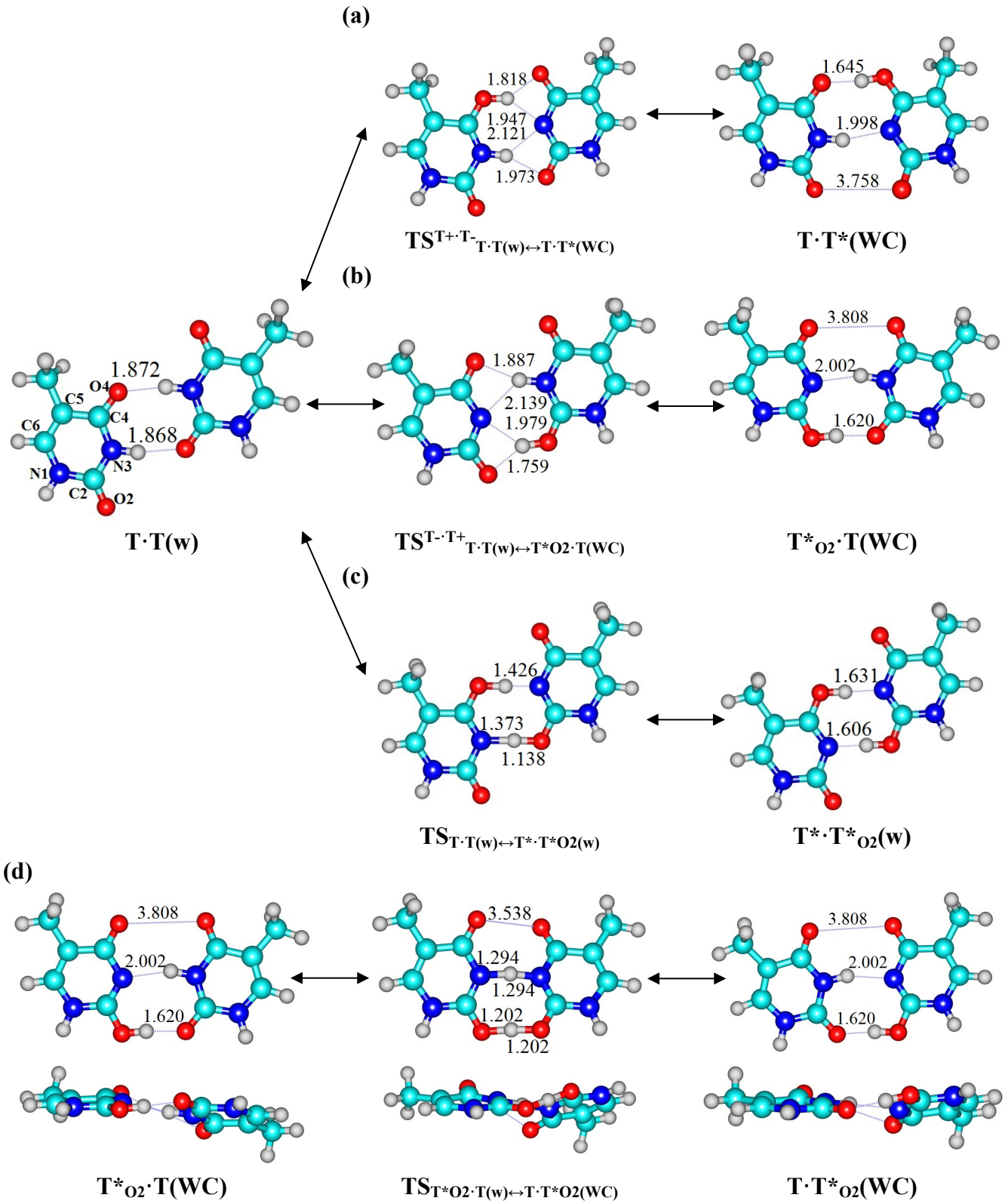

Fig. S1. Structures of the stationary points of the (a) T·T(w)↔T·T*(WC), (b) T·T(w)↔T*$_{O2}$·T(WC), (c) T·T(w)↔T*·T*$_{O2}$(w) and (d) T*$_{O2}$·T(w)↔T·T*$_{O2}$(WC) conversions *via* the sequential DPT accompanied by the structural rearrangement of the base pair obtained at the B3LYP/6-311++G(d,p) level of theory. Dotted lines indicate AH···B H-bonds and attractive A···B van der Waals contacts (their lengths are presented in angstroms), while continuous – covalent bonds; carbon atoms are in light-blue, nitrogen – in dark-blue, hydrogen – in grey and oxygen – in red.

Table S4. Energetic and kinetic characteristics (WC) (ν_i=1249.5*i* cm^{-1}), T·T(w)↔T*$_{O2}$·T(WC), T*$_{O2}$·T(w)↔T·T*$_{O2}$(WC) and T·T(w)↔T*·T*$_{O2}$(w) tautomerisations *via* the sequential DPT obtained at the different levels of theory for the geometry calculated at the B3LYP/6-311++G(d,p) level of theory (see also Figs. 1 and S1).

Level of theory	ΔG^a	ΔE^b	$\Delta\Delta G_{TS}^c$	$\Delta\Delta E_{TS}^d$	$\Delta\Delta G^e$	$\Delta\Delta E^f$	$\tau_{99.9\%}^g$
T·T(w)↔T·T*(WC) (ν_i=274.5*i* cm^{-1})							
MP2/6-311++G(2df,pd)	8.82	8.49	31.18	32.02	22.36	23.53	$2.62\cdot10^{4}$
MP2/6-311++G(3df,2pd)	9.18	8.85	31.20	32.03	22.01	23.19	$1.46\cdot10^{4}$
MP2/cc-pVTZ	8.76	8.43	31.27	32.10	22.51	23.68	$3.36\cdot10^{4}$
MP2/cc-pVQZ	8.98	8.64	31.06	31.90	22.09	23.26	$1.65\cdot10^{4}$
T·T(w)↔T*$_{O2}$·T(WC) (ν_i=278.5*i* cm^{-1})							
MP2/6-311++G(2df,pd)	12.68	12.77	32.95	34.08	20.27	21.31	$7.63\cdot10^{2}$
MP2/6-311++G(3df,2pd)	12.91	13.00	33.01	34.15	20.10	21.14	$5.74\cdot10^{2}$
MP2/cc-pVTZ	12.57	12.66	32.98	34.11	20.41	21.45	$9.70\cdot10^{2}$
MP2/cc-pVQZ	12.72	12.81	32.82	33.96	20.11	21.15	$5.82\cdot10^{2}$
MP2/6-311++G(2df,pd)	0.00	0.00	3.74	6.90	3.74	6.90	$1.28\cdot10^{-10}$
MP2/6-311++G(3df,2pd)	0.00	0.00	4.24	7.41	4.24	7.41	$2.99\cdot10^{-10}$
MP2/cc-pVTZ	0.00	0.00	4.10	7.26	4.10	7.26	$2.34\cdot10^{-10}$
MP2/cc-pVQZ	0.00	0.00	4.40	7.56	4.40	7.56	$3.88\cdot10^{-10}$
T·T(w)↔T*·T*$_{O2}$(w) (ν_i=661.4*i* cm^{-1})							
MP2/6-311++G(2df,pd)	15.17	15.55	13.14	16.34	-2.04	0.79	$2.56\cdot10^{-14}$
MP2/6-311++G(3df,2pd)	15.77	16.15	13.89	17.10	-1.88	0.94	$3.32\cdot10^{-14}$
MP2/cc-pVTZ	15.36	15.74	13.47	16.68	-1.89	0.93	$3.26\cdot10^{-14}$
MP2/cc-pVQZ	15.61	15.99	13.82	17.03	-1.79	1.03	$3.88\cdot10^{-14}$

[a]The Gibbs free energy of the product relatively the reactant of the tautomerisation reaction (T=298.15 K), kcal·mol^{-1}

[b]The electronic energy of the product relatively the reactant of the tautomerisation reaction, kcal·mol^{-1}

[c]The Gibbs free energy barrier for the forward reaction of tautomerisation, kcal·mol^{-1}

[d]The electronic energy barrier for the forward reaction of tautomerisation, kcal·mol^{-1}

[e]The Gibbs free energy barrier for the reverse reaction of tautomerisation, kcal·mol^{-1}

[f]The electronic energy barrier for the reverse reaction of tautomerisation, kcal·mol^{-1}

[g]The time necessary to reach 99.9% of the equilibrium concentration between the reactant and the product of the tautomerisation reaction, s

ν_i – imaginary frequency.

See also summary Table S2 for the Gibbs and electronic energies of the mispairs and TSs relatively the global minimum – the T·T(w) DNA base mispair.

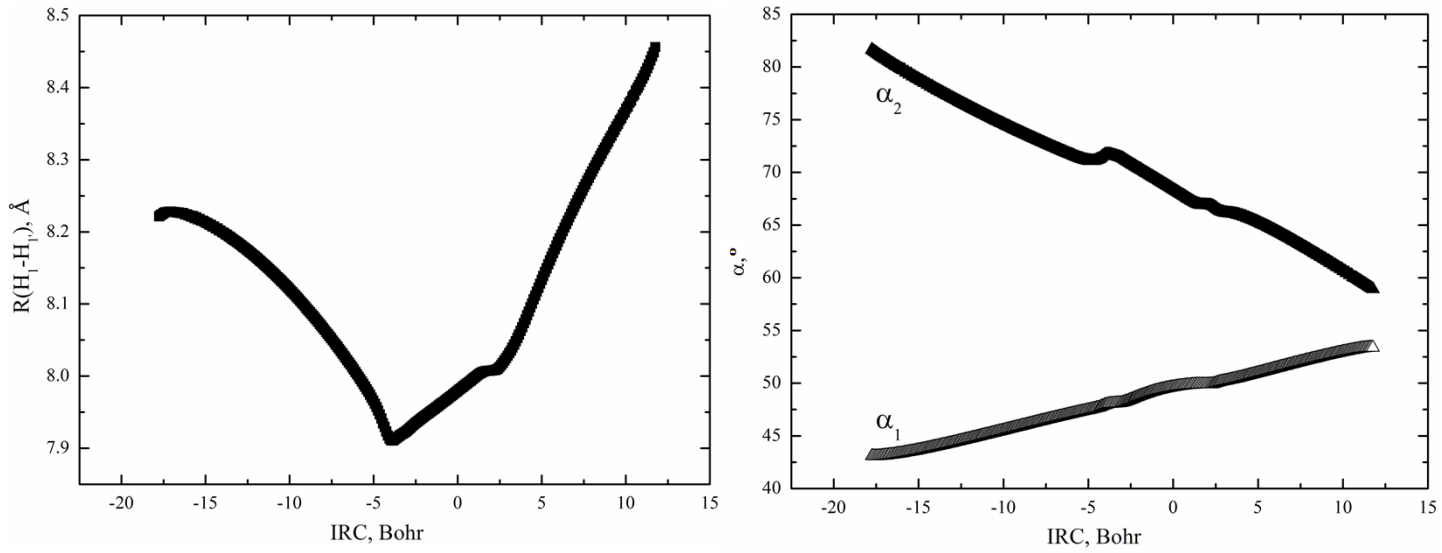

(**a**) (**b**)

Fig. S2. Profiles of: (**a**) the $R(H_1\text{-}H_{1'})$ distances between the H_1 and $H_{1'}$ glycosidic hydrogens and (**b**) the $\alpha_1=\angle N1H_1H_{1'}$ (angle for the base on the left within the base pair) or $\alpha_2=\angle N1H_{1'}H_1$ (angle for the base on the right within the base pair) glycosidic angles along the IRC of the T·T(w)↔T·T*(WC) tautomerisation *via* the sequential DPT obtained at the B3LYP/6-311++G(d,p) level of theory (see also Figs. 1 and S1).

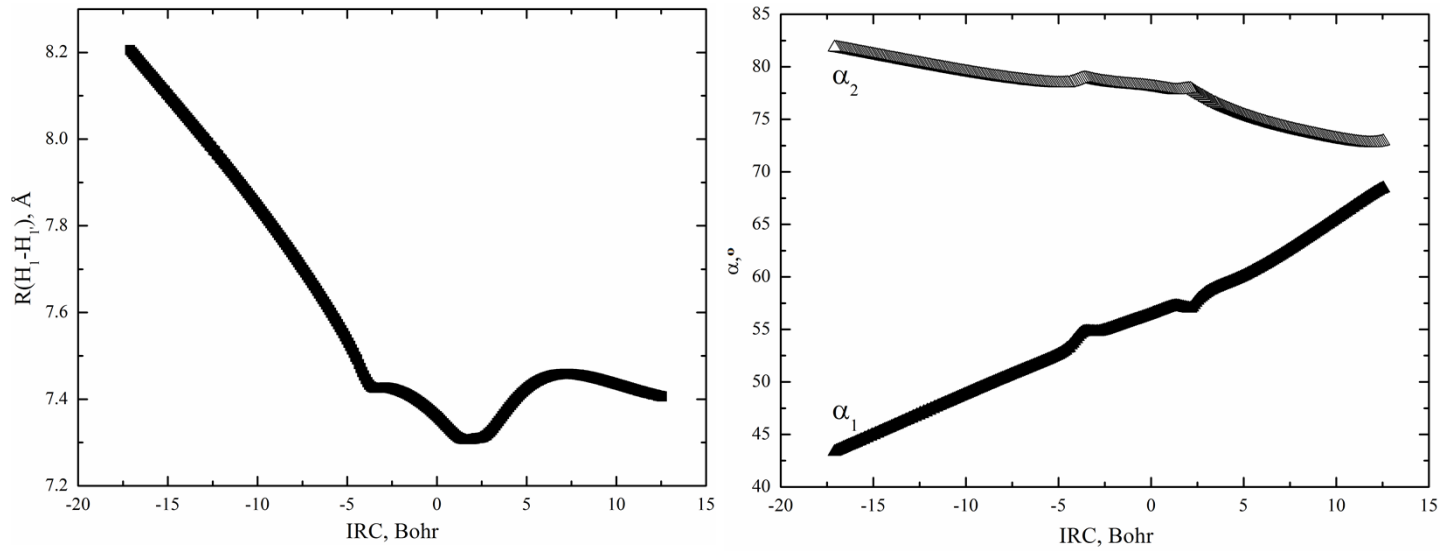

(**a**) (**b**)

Fig. S3. Profiles of: (**a**) the $R(H_1\text{-}H_{1'})$ distances between the H_1 and $H_{1'}$ glycosidic hydrogens and (**b**) the $\alpha_1=\angle N1H_1H_{1'}$ (angle for the base on the left within the base pair) or $\alpha_2=\angle N1H_{1'}H_1$ (angle for the base on the right within the base pair) glycosidic angles along the IRC of the T·T(w)↔T*$_{O2}$·T(WC) tautomerisation *via* the sequential DPT obtained at the B3LYP/6-311++G(d,p) level of theory (see Figs. 1 and S1).

Table S5. Patterns of the specific intermolecular interactions including AH···B H-bonds, attractive O/N···O van der Waals contacts and loosened A-H-B covalent bridges that sequentially replace each other along the IRC of the T·T(w)↔T·T*(WC) and T·T(w)↔T*$_{O2}$·T(WC) tautomerisations *via* the sequential DPT and ranges of their existence obtained at the B3LYP/6-311++G(d,p) level of theory (see also Figs. 1, 2 and S1).

Patterns	IRC range, Bohr	Intermolecular interactions, forming patterns
T·T(w)↔T·T*(WC)		
I	[-17.75÷-4.44)	N3H···O4, N3H···O2
II	[-4.44÷-3.28)	N3H···O4, N3H···N3, N3H···O2
III	[-3.28÷-2.80)	N3-H-O4, N3H···N3, N3H···O2
IV	[-2.80÷-1.16)	O4H···N3, N3H···N3, N3H···O2
V	[-1.16÷0.68)	O4H···O4, O4H···N3, N3H···N3, N3H···O2
VI	[0.68÷1.54)	O4H···O4, N3H···N3, N3H···O2
VII	[1.54÷1.83)	O4-H-O4, N3H···N3, N3H···O2
VIII	[1.83÷2.88)	O4H···O4, N3H···N3, N3H···O2
IX	[2.88÷4.62)	O4H···O4, N3H···N3, N3H···O2, N3···O4
X	[4.62÷4.82)	O4H···O4, N3H···N3, N3H···O2, N3···O4, O2···O2
XI	[4.82÷4.91)	O4H···O4, N3H···N3, N3H···O2, O2···O2
XII	[4.91÷11.76]	O4H···O4, N3H···N3, O2···O2
T·T(w)↔T*$_{O2}$·T(WC)		
I	[-17.09÷-4.44)	N3H···O4, N3H···O2
II	[-4.44÷-3.19)	N3H···O4, N3H···N3, N3H···O2
III	[-3.19÷-2.80)	N3H···O4, N3H···N3, N3-H-O2
IV	[-2.80÷-1.25)	N3H···O4, N3H···N3, O2H···N3
V	[-1.25÷0.38)	N3H···O4, N3H···N3, O2H···N3, O2H···O2
VI	[0.38÷1.35)	N3H···O4, N3H···N3, O2H···O2
VII	[1.35÷1.64)	N3H···O4, N3H···N3, O2-H-O2
VIII	[1.64÷2.40)	N3H···O4, N3H···N3, O2H···O2
IX	[2.40÷5.59)	N3H···O4, N3H···N3, N3···O2, O2H···O2
X	[5.59÷12.54]	O4···O4, N3H···N3, O2H···O2

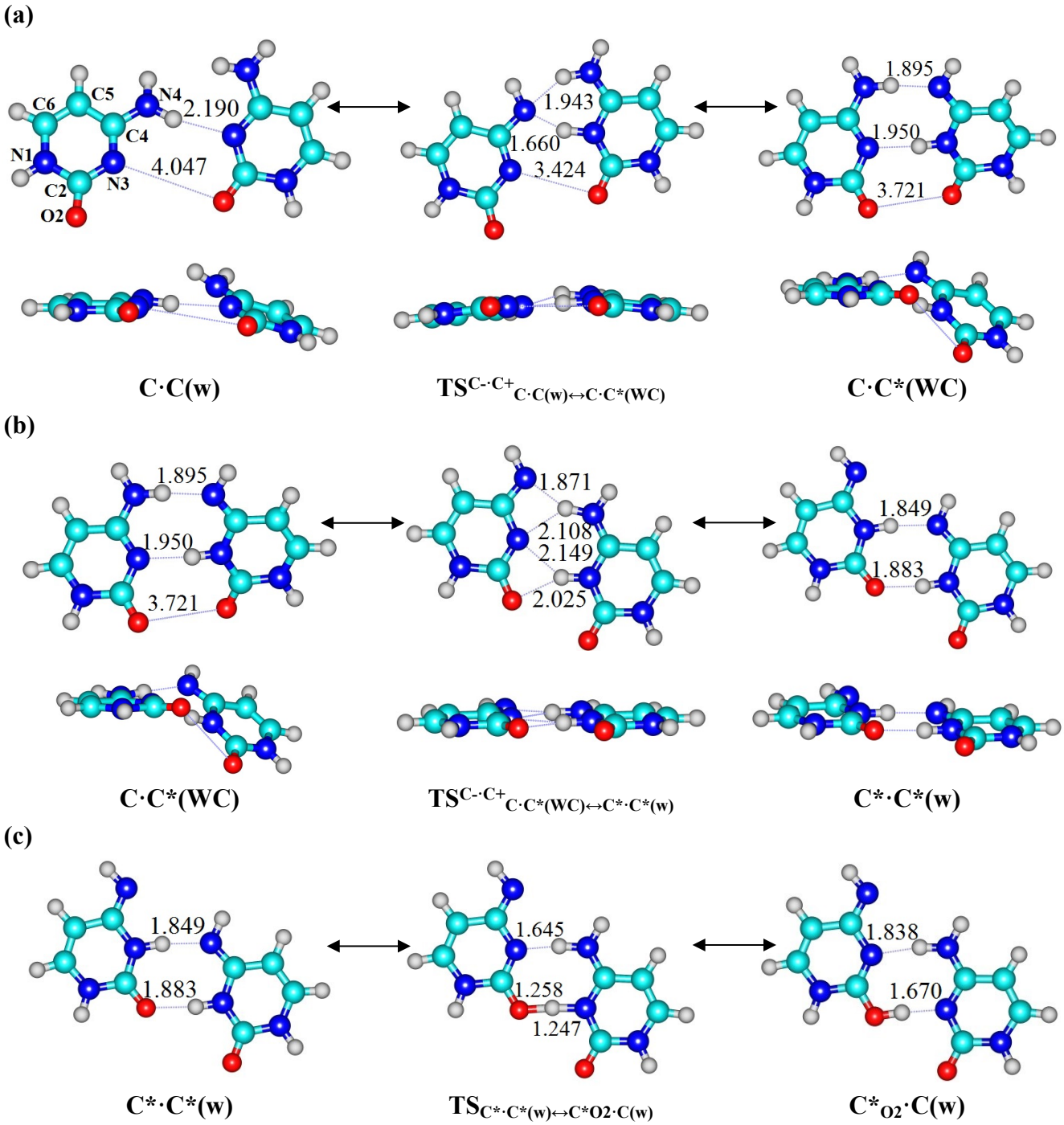

Fig. S4. Structures of the stationary points of the (**a**) C·C(w)↔C·C*(WC), (**b**) C·C*(WC)↔C*·C*(w) and (**c**) C*·C*(w)↔C*$_{O2}$·C(w) conversions *via* the sequential DPT accompanied by the structural rearrangement of the base pair obtained at the B3LYP/6-311++G(d,p) level of theory. For the designations see Fig. S1.

Table S6. Energetic and kinetic characteristics of the C·C(w)↔C·C*(WC), C·C*(WC)↔C*·C*(w) and C*·C*(w)↔C*$_{O2}$·C(w) tautomerisations *via* the sequential DPT obtained at the different levels of theory for the geometry calculated at the B3LYP/6-311++G(d,p) level of theory (see also Figs. 4 and S4).

Level of theory	ΔG	ΔE	$\Delta\Delta G_{TS}$	$\Delta\Delta E_{TS}$	ΔΔG	ΔΔE	$\tau_{99.9\%}$
C·C(w)↔C·C*(WC) (ν_i=239.0*i* cm^{-1})							
MP2/6-311++G(2df,pd)	-9.06	-10.89	25.25	24.19	34.31	35.08	$3.50\cdot10^{6}$
MP2/6-311++G(3df,2pd)	-9.05	-10.88	25.09	24.04	34.15	34.92	$2.69\cdot10^{6}$
MP2/cc-pVTZ	-9.25	-11.08	25.70	24.64	34.95	35.73	$7.50\cdot10^{6}$
MP2/cc-pVQZ	-8.90	-10.73	25.38	24.32	34.28	35.05	$4.35\cdot10^{6}$
C·C*(WC)↔C*·C*(w) (ν_i=162.0*i* cm^{-1})							
MP2/6-311++G(2df,pd)	1.61	1.77	18.59	19.69	16.98	17.92	2.89
MP2/6-311++G(3df,2pd)	1.31	1.47	18.19	19.29	16.88	17.82	2.36
MP2/cc-pVTZ	1.28	1.44	18.78	19.89	17.50	18.45	6.74
MP2/cc-pVQZ	1.34	1.50	18.34	19.44	17.00	17.94	2.90
MP2/6-311++G(2df,pd)	5.81	6.11	6.04	8.73	0.23	2.61	$1.02\cdot10^{-12}$
MP2/6-311++G(3df,2pd)	6.14	6.44	6.52	9.21	0.38	2.77	$1.33\cdot10^{-12}$
MP2/cc-pVTZ	6.20	6.50	6.75	9.43	0.55	2.93	$1.75\cdot10^{-12}$
MP2/cc-pVQZ	6.07	6.36	6.59	9.27	0.53	2.91	$1.69\cdot10^{-12}$

For the designations see Table S4.

See also summary Table S2 for the Gibbs and electronic energies of the mispairs and TSs relatively the global minimum – the C·C*(WC) DNA base mispair.

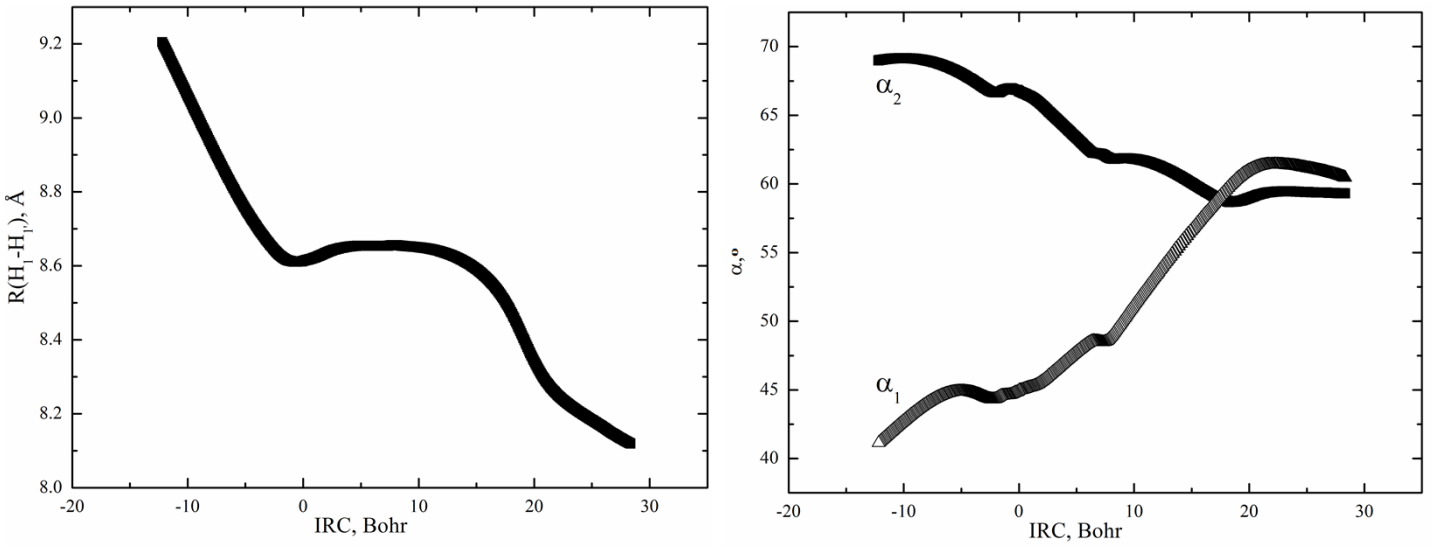

(**a**) (**b**)

Fig. S5. Profiles of: (**a**) the $R(H_1\text{-}H_{1'})$ distances between the H_1 and $H_{1'}$ glycosidic hydrogens and (**b**) the $\alpha_1=\angle N1H_1H_{1'}$ (angle for the base on the left within the base pair) or $\alpha_2=\angle N1H_{1'}H_1$ (angle for the base on the right within the base pair) glycosidic angles along the IRC of the C·C(w)↔C·C*(WC) tautomerisation *via* the sequential DPT obtained at the B3LYP/6-311++G(d,p) level of theory (see Figs. 4 and S4).

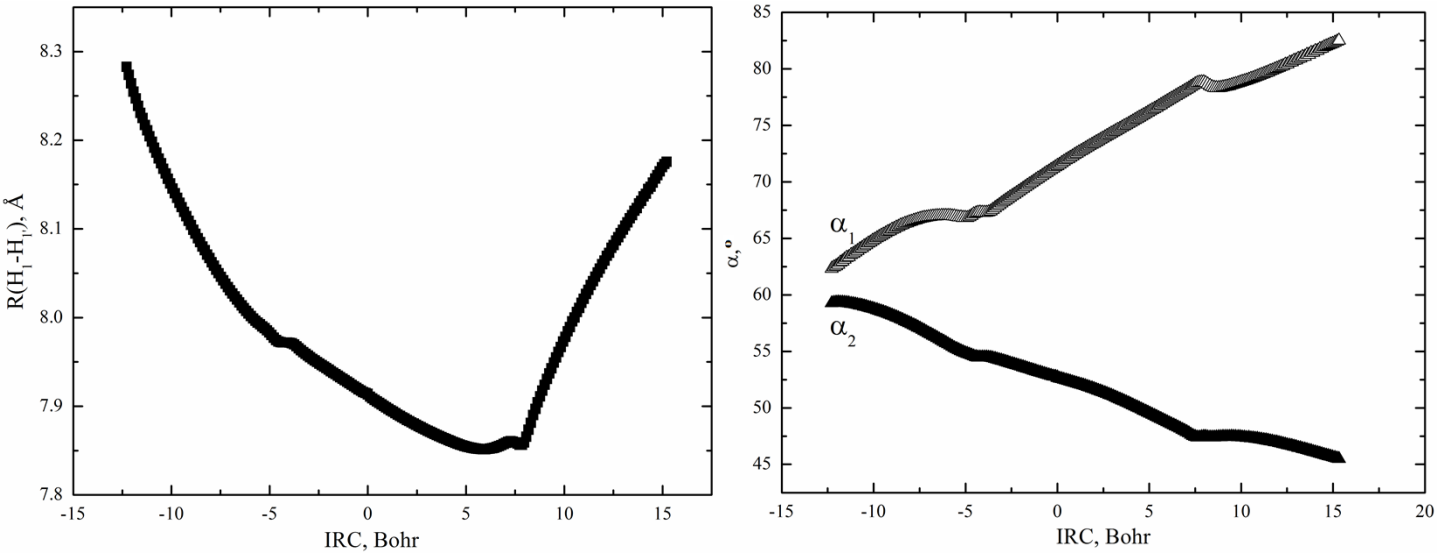

(**a**) (**b**)

Fig. S6. Profiles of: (**a**) the $R(H_1\text{-}H_{1'})$ distances between the H_1 and $H_{1'}$ glycosidic hydrogens and (**b**) the $\alpha_1=\angle N1H_1H_{1'}$ (angle for the base on the left within the base pair) or $\alpha_2=\angle N1H_{1'}H_1$ (angle for the base on the right within the base pair) glycosidic angles along the IRC of the C·C*(WC)↔C*·C*(w) tautomerisation *via* the sequential DPT obtained at the B3LYP/6-311++G(d,p) level of theory (see Figs. 4 and S4).

Table S7. Patterns of the specific intermolecular interactions including AH···B, AH···HB H-bonds, attractive O/N···O van der Waals contact and loosened A-H-B covalent bridges that sequentially replace each other along the IRC of the C·C(w)↔C·C*(WC) and C·C*(WC)↔C*·C*(w) tautomerisations *via* the sequential DPT accompanied by the structural rearrangement of the base pair and ranges of their existence obtained at the B3LYP/6-311++G(d,p) level of theory (see Figs. 4, 5 and S4).

Patterns	IRC range, Bohr	Intermolecular interactions, forming patterns
C·C(w)↔C·C*(WC)		
I	[-12.19÷-7.98)	N4H···N3, N3···O2
II	[-7.98÷-1.13)	N4H···N4, N4H···N3, N3···O2
III	[-1.13÷-0.69)	N4H···N4, N4-H-N3, N3···O2
IV	[-0.69÷3.98)	N4H···N4, N3H···N4, N3···O2
V	[3.98÷4.16)	N4H···N4, N3H···N4
VI	[4.16÷6.18)	N4H···N4, N3H···N4, N3H···N3
VII	[6.18÷6.70)	N4-H-N4, N3H···N4, N3H···N3
VIII	[6.70÷7.14)	N4H···N4, N3H···N4, N3H···N3
IX	[7.14÷9.25)	N4H···N4, N3H···HN4, N3H···N3
X	[9.25÷12.67)	N4H···N4, N3H···N3
XI	[12.67÷28.34]	N4H···N4, N3H···N3, O2···O2
C·C*(WC)↔C*·C*(w)		
I	[-12.28÷-4.10)	N4H···N4, N3H···N3, O2···O2
II	[-4.10÷-3.63)	N4-H-N4, N3H···N3, O2···O2
III	[-3.63÷-2.34)	N4H···N4, N3H···N3, O2···O2
IV	[-2.34÷-1.05)	N4H···N4, N3H···N3, N3H···O2, O2···O2
V	[-1.05÷-0.47)	N4H···N4, N4H···N3, N3H···N3, N3H···O2, O2···O2
VI	[-0.47÷1.88)	N4H···N4, N4H···N3, N3H···N3, N3H···O2
VII	[1.88÷2.70)	N4H···N4, N4H···N3, N3H···O2
VIII	[2.70÷7.15)	N4H···N3, N3H···O2
IX	[7.15÷7.73)	N4-H-N3, N3H···O2
X	[7.73÷15.32]	N3H···N4, N3H···O2

3. References.

1. Frisch, M.J., Trucks, G.W., Schlegel, H.B., Scuseria, G.E., Robb, M.A., & Cheeseman, J.R., … Pople, J.A. (2010). *GAUSSIAN 09* (Revision B.01). Wallingford CT: Gaussian Inc.
2. Tirado-Rives, J., & Jorgensen, W.L. (2008). Performance of B3LYP Density Functional Methods for a large set of organic molecules. *Journal of Chemical Theory and Computation*, *4,* 297–306.
3. Parr, R.G., & Yang, W. (1989). *Density-functional theory of atoms and molecules*. Oxford: Oxford University Press.
4. Lee, C., Yang, W., & Parr, R.G. (1988). Development of the Colle-Salvetti correlation-energy formula into a functional of the electron density. *Physical Review B: Condensed Matter and Materials Physics*, *37*, 785-789.
5. Matta, C.F. (2010). How dependent are molecular and atomic properties on the electronic structure method? Comparison of Hartree-Fock, DFT, and MP2 on a biologically relevant set of molecules. *Journal of Computational Chemistry, 31*, 1297–1311.
6. Brovarets', O.O., Zhurakivsky, R.O., & Hovorun, D.M. (2013). The physico-chemical mechanism of the tautomerisation *via* the DPT of the long Hyp*·Hyp Watson-Crick base pair containing rare tautomer: a QM and QTAIM detailed look. *Chemical Physics Letters*, *578*, 126-132.
7. Brovarets', O.O., & Hovorun, D.M. (2013). Atomistic understanding of the C·T mismatched DNA base pair tautomerization *via* the DPT: QM and QTAIM computational approaches. *Journal of Computional Chemistry, 34*, 2577-2590.
8. Brovarets', O.O., Zhurakivsky, R.O., & Hovorun, D.M. (2014). Is the DPT tautomerisation of the long A·G Watson-Crick DNA base mispair a source of the adenine and guanine mutagenic tautomers? A QM and QTAIM response to the biologically important question. *Journal of Computational Chemistry, 35*, 451-466.
9. Samijlenko, S.P., Yurenko, Y.P., Stepanyugin, A.V., & Hovorun, D.M. (2012). Tautomeric equilibrium of uracil and thymine in model protein−nucleic acid contacts. Spectroscopic and quantum chemical approach. *Journal of Physical Chemistry B, 114*, 1454-1461.
10. Peng, C., Ayala, P.Y., Schlegel, H.B., & Frisch, M.J. (1996). Using redundant internal coordinates to optimize equilibrium geometries and transition states. *Journal of Computational Chemistry, 17*, 49–56.
11. Frisch, M.J., Head-Gordon, M., & Pople, J.A. (1990). Semi-direct algorithms for the MP2 energy and gradient. *Chemical Physics Letters, 166,* 281-289.
12. Hariharan, P.C., & Pople, J.A. (1973). The influence of polarization functions on molecular orbital hydrogenation energies. *Theoretical Chemistry Accounts: Theory, Computation, and Modeling (Theoretica Chimica Acta), 28*, 213−222.
13. Krishnan, R., Binkley, J.S., Seeger, R., & Pople, J.A. (1980). Self-consistent molecular orbital methods. XX. A basis set for correlated wave functions. *Journal of Chemical Physics, 72*, 650−654.
14. Kendall, R.A., Dunning, Jr., T.H., & Harrison, R.J. (1992). Electron affinities of the first-row atoms revisited. Systematic basis sets and wave functions. *Journal of Chemical Physics, 96*, 6796−6806.
15. Hratchian, H.P., & Schlegel, H.B. (2005). Finding minima, transition states, and following reaction pathways on ab initio potential energy surfaces. In Dykstra, C.E., Frenking, G., Kim, K.S., & Scuseria, G. (Eds.), *Theory and applications of computational chemistry: The first 40 years* (pp. 195-249). Amsterdam: Elsevier.
16. Brovarets', O.O., Zhurakivsky, R.O., & Hovorun, D.M. (2015). DPT tautomerisation of the wobble guanine·thymine DNA base mispair is not mutagenic: QM and QTAIM arguments. *Journal of Biomolecular Structure and Dynamics,* 33, 674-689.
17. Brovarets', O.O., Zhurakivsky, R.O., & Hovorun, D.M. (2013). The physico-chemical "anatomy" of the tautomerisation through the DPT of the biologically important pairs of hypoxanthine with DNA bases: QM and QTAIM perspectives. *Journal of Molecular Modeling*, *19*, 4119-4137.
18. Boys, S.F., & Bernardi, F. (1970). The calculation of small molecular interactions by the differences of separate total energies. Some procedures with reduced errors. *Molecular Physics*, *19,* 553–566.
19. Gutowski, M., Van Lenthe, J.H., Verbeek, J., Van Duijneveldt, F.B., & Chalasinski, G. (1986). The basis set superposition error in correlated electronic structure calculations. *Chemical Physics Letters, 124,* 370–375.

20. Sordo, J.A., Chin, S., & Sordo, T.L. (1988). On the counterpoise correction for the basis set superposition error in large systems. *Theoretical Chemistry Accounts: Theory, Computation, and Modeling (Theoretica Chimica Acta), 74*, 101–110.
21. Sordo, J.A. (2001). On the use of the Boys–Bernardi function counterpoise procedure to correct barrier heights for basis set superposition error. *Journal of Molecular Structure: THEOCHEM, 537,* 245–251.
22. Atkins, P.W. (1998). *Physical chemistry*. Oxford: Oxford University Press.
23. Brovarets', O.O., & Hovorun, D.M. (2014). DPT tautomerisation of the G·A_{syn} and A*·G*$_{syn}$ DNA mismatches: A QM/QTAIM combined atomistic investigation. *Physical Chemistry Chemical Physics*, *16*, 9074-9085.
24. Bader, R.F.W. (1990). *Atoms in molecules: A quantum theory.* Oxford: Oxford University Press.
25. Matta, C.F. (2014). Modeling biophysical and biological properties from the characteristics of the molecular electron density, electron localization and delocalization matrices, and the electrostatic potential. *Journal of Computational Chemistry*, *35,* 1165-1198.
26. Lecomte, C., Espinosa, E., & Matta, C.F. (2015). On atom–atom 'short contact' bonding interactions in crystals. *IUCrJ, 2*, 161–163. doi: 10.1107/S2052252515002067.
27. Matta, C.F., Huang L., & Masaa, L. (2011). Characterization of a trihydrogen bond on the basis of the topology of the electron density. *Journal of Physical Chemistry A, 115*, 12451-12458.
28. Keith, T.A. (2010). *AIMAll* (Version 10.07.01). Retrieved from aim.tkgristmill.com.
29. Brovarets', O. O., Yurenko, Y. P., & Hovorun, D. M. (2014). Intermolecular CH···O/N H-bonds in the biologically important pairs of natural nucleobases: A thorough quantum-chemical study. *Journal of Biomolecular Structure & Dynamics, 32,* 993-1022.
30. Brovarets', O. O., Yurenko, Y. P., & Hovorun, D. M. (2015). The significant role of the intermolecular CH···O/N hydrogen bonds in governing the biologically important pairs of the DNA and RNA modified bases: a comprehensive theoretical investigation. *Journal of Biomolecular Structure & Dynamics, 33,* 1624-1652
31. Matta, C.F., Castillo, N., & Boyd, R.J. (2006). Extended weak bonding interactions in DNA: π-stacking (base-base), base-backbone, and backbone-backbone interactions. *Journal of Physical Chemistry B*, *110*, 563-578.
32. Espinosa, E., Molins, E., & Lecomte, C. (1998). Hydrogen bond strengths revealed by topological analyses of experimentally observed electron densities. *Chemical Physics Letters*, *285*, 170–173.
33. Mata, I., Alkorta, I., Espinosa, E., & Molins, E. (2011). Relationships between interaction energy, intermolecular distance and electron density properties in hydrogen bonded complexes under external electric fields. *Chemical Physics Letters, 507*, 185–189.
34. Iogansen, A.V. (1999). Direct proportionality of the hydrogen bonding energy and the intensification of the stretching *ν*(XH) vibration in infrared spectra. *Spectrochimica Acta Part A: Molecular and Biomolecular Spectroscopy, 55,* 1585–1612.
35. Nikolaienko, T.Y., Bulavin, L.A., & Hovorun, D.M. (2012). Bridging QTAIM with vibrational spectroscopy: The energy of intramolecular hydrogen bonds in DNA-related biomolecules. *Physical Chemistry Chemical Physics, 14*, 7441–7447.
36. Saenger, W. (1984). *Principles of nucleic acid structure.* New York: Springer.
37. Brovarets', O.O., Zhurakivsky, R.O., & Hovorun, D.M. (2014). Structural, energetic and tautomeric properties of the T·T*/T*·T DNA mismatch involving mutagenic tautomer of thymine: A QM and QTAIM insight. *Chemical Physics Letters*, *592,* 247-255.
38. Brovarets', O.O., & Hovorun, D.M. (2013). Atomistic nature of the DPT tautomerisation of the biologically important C•C* DNA base mispair containing amino and imino tautomers of the cytosine: A QM and QTAIM approach. *Physical Chemistry Chemical Physics, 15*, 20091-20104.